LETTER

Global land change from 1982 to 2016

Xiao-Peng Song[1]*, Matthew C. Hansen[1], Stephen V. Stehman[2], Peter V. Potapov[1], Alexandra Tyukavina[1], Eric F. Vermote[3] & John R. Townshend[1]

Land change is a cause and consequence of global environmental change[1,2]. Changes in land use and land cover considerably alter the Earth's energy balance and biogeochemical cycles, which contributes to climate change and—in turn—affects land surface properties and the provision of ecosystem services[1–4]. However, quantification of global land change is lacking. Here we analyse 35 years' worth of satellite data and provide a comprehensive record of global land-change dynamics during the period 1982–2016. We show that—contrary to the prevailing view that forest area has declined globally[5]—tree cover has increased by 2.24 million km^2 (+7.1% relative to the 1982 level). This overall net gain is the result of a net loss in the tropics being outweighed by a net gain in the extratropics. Global bare ground cover has decreased by 1.16 million km^2 (−3.1%), most notably in agricultural regions in Asia. Of all land changes, 60% are associated with direct human activities and 40% with indirect drivers such as climate change. Land-use change exhibits regional dominance, including tropical deforestation and agricultural expansion, temperate reforestation or afforestation, cropland intensification and urbanization. Consistently across all climate domains, montane systems have gained tree cover and many arid and semi-arid ecosystems have lost vegetation cover. The mapped land changes and the driver attributions reflect a human-dominated Earth system. The dataset we developed may be used to improve the modelling of land-use changes, biogeochemical cycles and vegetation–climate interactions to advance our understanding of global environmental change[1–4,6].

Humanity depends on land for food, energy, living space and development. Land-use change—traditionally a local-scale human practice—is increasingly affecting Earth system processes, including the surface energy balance, the carbon cycle, the water cycle and species diversity[1–4]. Land-use change is estimated to have contributed a quarter of cumulative carbon emissions to the atmosphere since industrialization[3]. As population and per capita consumption continue to grow, so does demand for food, natural resources and consequent stress to ecosystems.

Because of their synoptic view and recurrent monitoring of the Earth's surface, satellite observations contribute substantially to our current understanding of the global extent and change of land cover and land use. Previous global-scale studies have mainly focused on annual forest cover change (stand-replacement disturbance) for the time period after 2000[7], or focused on sparse temporal intervals[8]. Long-term gradual changes in undisturbed forests as well as areal changes in cropland, grassland and other non-forested land are less well quantified.

We create an annual, global vegetation continuous fields product[9] for the time period 1982 to 2016, consisting of tall vegetation (≥5 m in height; hereafter referred to as tree canopy (TC)) cover, short vegetation (SV) cover and bare ground (BG) cover, at 0.05°× 0.05° spatial resolution (for details of definitions, see Supplementary Methods). For each year, every land pixel is characterized by its per cent cover of TC, SV and BG, representing the vegetation composition at the time of the local peak growing season. The dataset is produced by combining optical observations from multiple satellite sensors, including the Advanced Very High Resolution Radiometer (AVHRR), the Moderate Resolution

Imaging Spectroradiometer, the Landsat Enhanced Thematic Mapper Plus and various sensors with very high spatial resolution. We use non-parametric trend analysis to detect and quantify changes in tree canopy, short vegetation and bare ground over the full time period at pixel (0.05° × 0.05°), regional and global scales. Observed changes are attributed to direct human activities or indirect drivers on the basis of a global probability sample and interpretation of high-resolution images from Google Earth.

The total area of tree cover increased by 2.24 million km^2 from 1982 to 2016 (90% confidence interval (CI): 0.93, 3.42 million km^2), which represents a +7.1% change relative to 1982 tree cover (Extended Data Table 1). Bare ground area decreased by 1.16 million km^2 (90% CI: −1.78, −0.34 million km^2), which represents a decrease of 3.1% relative to 1982 bare ground cover. The total area of short vegetation cover decreased by 0.88 million km^2 (90% CI: −2.20, 0.52 million km^2), which indicates a decrease of 1.4% relative to 1982 short vegetation cover. A global net gain in tree canopy contradicts current understanding of long-term forest area change; the Food and Agriculture Organization of the United Nations (FAO) reported a net forest loss between 1990 and 2015[5]. However, our gross tree canopy loss estimate (−1.33 million km^2, −4.2%, Extended Data Table 1) agrees in magnitude with the FAO's estimate of net forest area change (−1.29 million km^2, −3%), despite differences in the time period covered and definition of forest (the FAO defines 'forest' as tree cover ≥10%; see details in Supplementary Methods).

The mapped land change (Fig. 1) consists of all changes in land cover and land use induced by natural or anthropogenic drivers. Land change themes are also inherently linked in the tree cover–short vegetation–bare ground nexus. For example, deforestation for agricultural expansion is often manifested as tree canopy loss and short vegetation gain, whereas land degradation may simultaneously result in short vegetation loss and bare ground gain. Pairs of changes in TC (ΔTC), SV (ΔSV) and BG (ΔBG) show strong coupling and symmetry in change direction but vary substantially over space (Fig. 1b and Extended Data Fig. 1). That is, the globally dominant, coupled land changes are ΔTC co-located with ΔSV and ΔSV co-located with ΔBG.

The overall net gain in tree canopy is a result of a net loss in the tropics being outweighed by a net gain in the subtropical, temperate and boreal climate zones (Extended Data Table 2). A latitudinal north (gain)–south (loss) contrast in tree cover change is evident (Fig. 2a). Conversely, for short vegetation tropical net gain is exceeded by extratropical net loss. The latitudinal profile of ΔSV largely mirrors that of ΔTC, most obviously in the northern mid-to-high latitudes (45° N–75° N) and low latitudes (30° S–10° N) (Fig. 2b). For bare ground, subtropical net gain partially offsets losses in all other climate domains. In the northern low-to-mid latitudes (10° N–45° N), the profile of bare ground loss (Fig. 2c) closely corresponds to that of short vegetation gain (Fig. 2b).

Changes were unevenly distributed across biomes (Fig. 3, Extended Data Fig. 2 and Extended Data Table 2). The largest area of net tree canopy loss occurred in the tropical dry forest biome (−95,000 km^2, −8%) (Extended Data Fig. 2a), closely followed by tropical moist deciduous forest (−84,000 km^2, −2%) (Fig. 3c) (all per cent net changes

[1]Department of Geographical Sciences, University of Maryland, College Park, MD, USA. [2]College of Environmental Science and Forestry, State University of New York, Syracuse, NY, USA. [3]NASA Goddard Space Flight Center, Greenbelt, MD, USA. *e-mail: xpsong@umd.edu
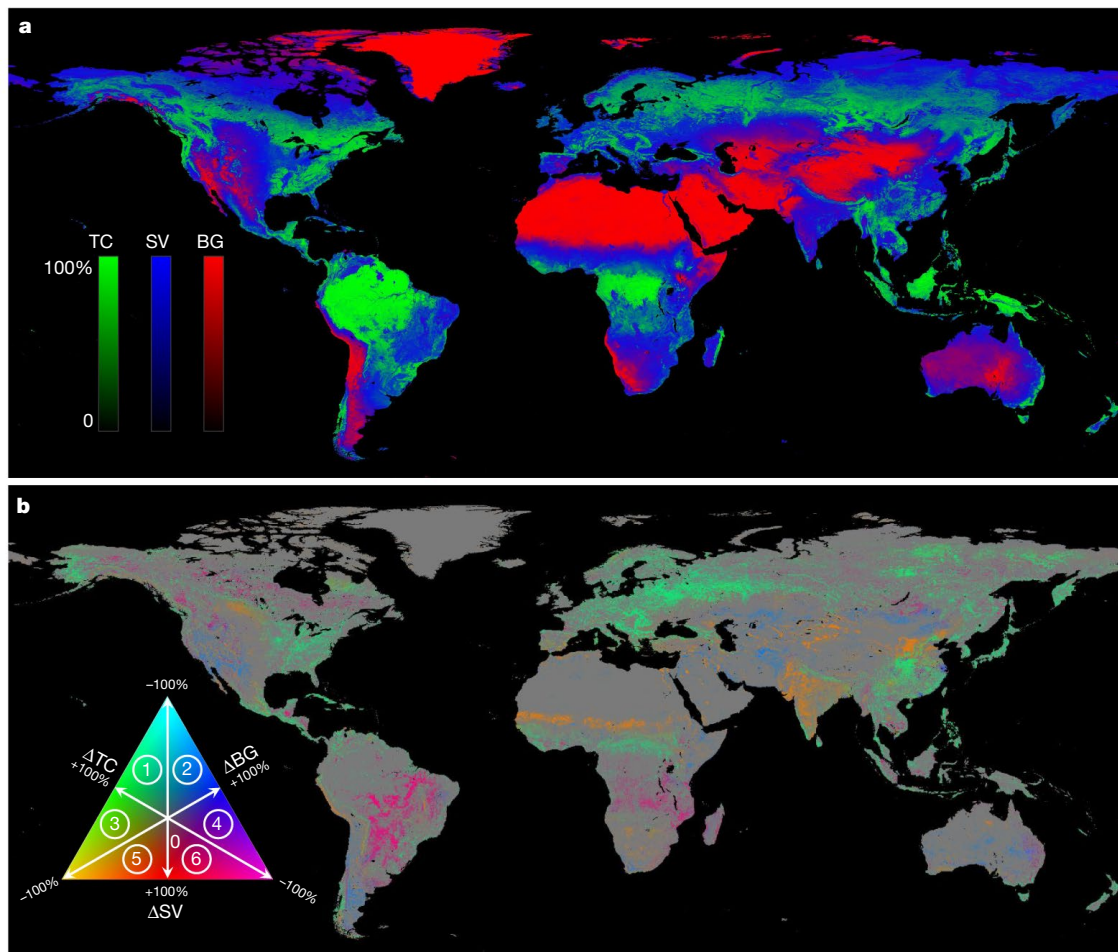
Fig. 1 | A satellite-based record of global TC, SV and BG cover from 1982 to 2016. a, Mean annual estimates. **b**, Long-term change estimates. Both mean and change estimates are expressed as per cent of pixel area at 0.05° × 0.05° spatial resolution. Pixels showing a statistically significant trend ($n = 35$, two-sided Mann–Kendall test, $P < 0.05$) in either TC, SV or BG are depicted on the change map. Circled numbers in the colour legend denote dominant change directions: 1, TC gain with SV loss; 2, BG gain with SV loss; 3, TC gain with BG loss; 4, BG gain with TC loss; 5, SV gain with BG loss; and 6, SV gain with TC loss.

are expressed relative to the benchmark of the area of the cover class in 1982). Tree canopy in major forest biomes outside the tropics has increased over the past 35 years: temperate continental forest has experienced the largest gain (+726,000 km², +33%) (Fig. 3d), which is comparable to the next two biomes—boreal coniferous forest (+463,000 km², +12%) and subtropical humid forest (+280,000 km², +18%)—combined (Extended Data Fig. 2e, m).

Short vegetation loss mirrored tree cover gain dynamics, but with smaller magnitudes: temperate continental forest (−610,000 km², −14%), boreal coniferous forest (−430,000 km², −10%) and subtropical humid forest (−249,000 km², −9%). By contrast, tropical forest biomes all gained short vegetation, with tropical shrubland experiencing the largest areal increase (+417,000 km², +10%) (Fig. 3e), twice the amount of short vegetation gain in tropical dry forest (+246,000 km², +5%). Tropical shrubland also experienced the largest bare ground loss (−408,000 km², −10%). Subtropical desert—the second largest dryland biome on Earth—had the largest gain in bare ground (+154,000 km², +4%) (Fig. 3f), followed by subtropical steppe (+107,000 km², +5%) (Extended Data Fig. 2h).

Consistently across all climate domains, mountain systems experienced net bare ground loss, net short vegetation loss and net tree canopy gain (Extended Data Fig. 2c, f, i, n and Extended Data Table 2). In the high-latitude boreal tundra woodland and the polar ecozone (Extended Data Fig. 2o, p), bare ground decreased and tree canopy increased in both biomes, whereas short vegetation decreased in tundra woodland but increased in the polar ecozone.

Based on the data from the global probability sample, an estimated 60% of all changes were associated with direct human land-use activities and 40% with indirect drivers such as climate change (Extended Data Figs. 3, 4; see Supplementary Methods). Direct human impact varied from 36% for bare ground gain to 70% for tree canopy loss. At the
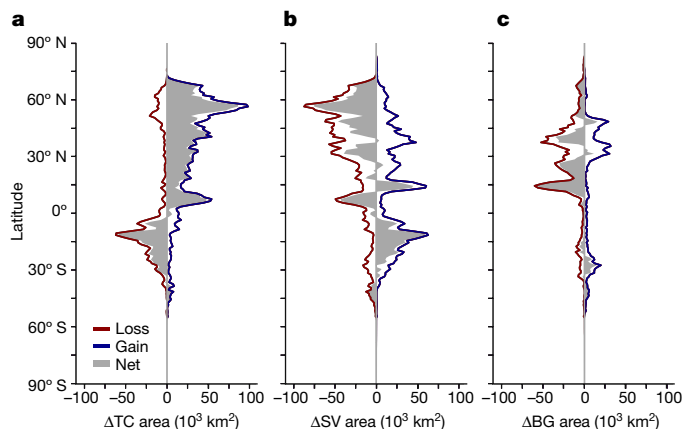

Fig. 2 | Latitudinal profiles of change in land cover from 1982 to 2016. a, Tree canopy cover change (ΔTC). **b**, Short vegetation cover change (ΔSV). **c**, Bare ground cover change (ΔBG). Area statistics were calculated for every 1° of latitude.
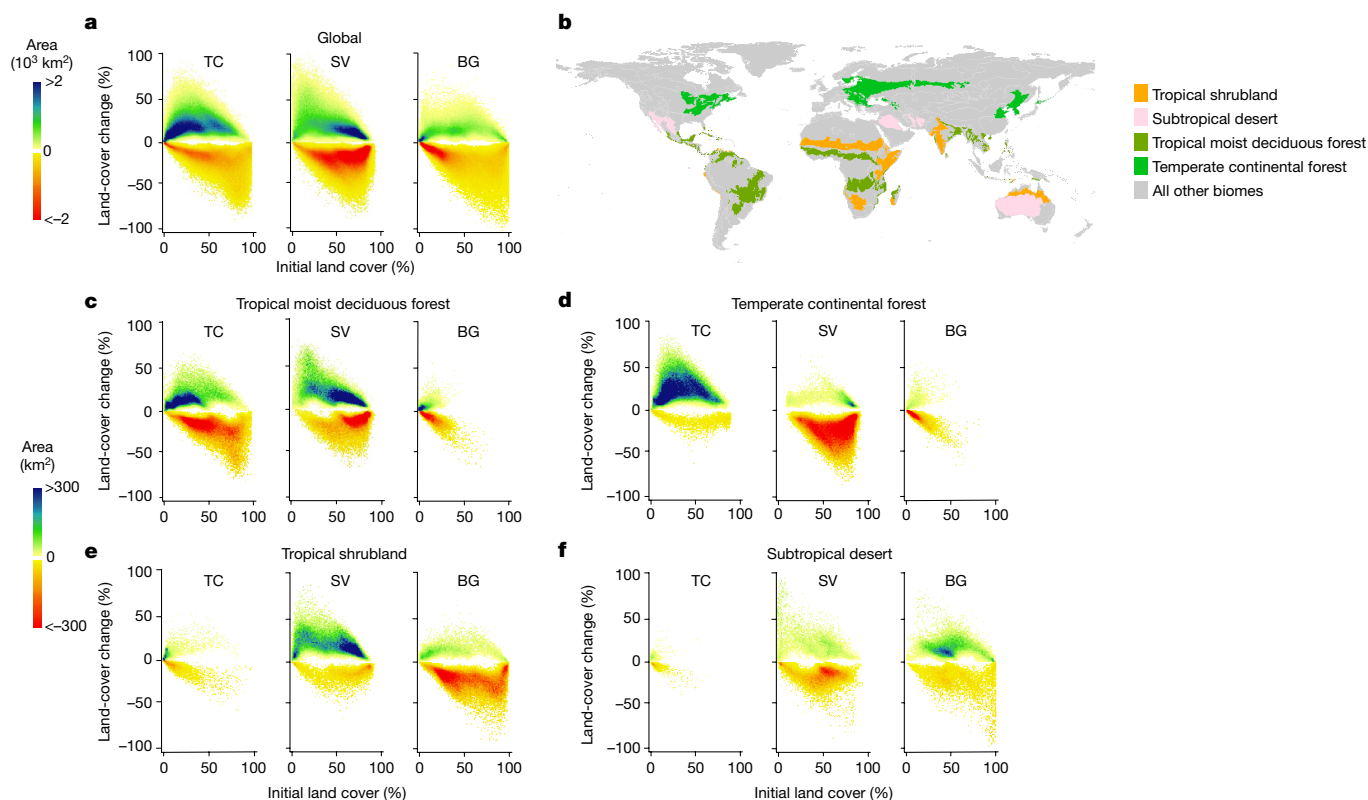
Fig. 3 | Intensity plots of gross area of loss and gain in TC, SV and BG cover during 1982–2016. a, Global-scale plots (top colour bar). Initial land cover (*x* axis) is defined as mean value of the first five years, 1982–1986. To create these plots, for each cover class, per cent change layer (Fig. 1b) and initial cover layer are used to construct a 2D histogram with bin size of 1% for both axes. Then, total change area in each bin is calculated and plotted. Data points located towards the lower-right corner of the TC plot are more likely to be deforestation (that is, points with large initial tree cover and large reduction in tree cover). The concentrated blue region of the SV plots reflects cropland intensification. The green belt on the BG plot suggests that vegetation loss occurred across the entire range

of BG coverage. The dominance of TC gain over TC loss, SV loss over SV gain and BG loss over BG gain are also clearly revealed. **b**, Geographical distribution of four highlighted biomes with largest gross areal changes. Biome distribution from a previous publication[30], reproduced with permission. **c**, Largest gross TC loss and SV gain. **d**, Largest gross TC gain and SV loss. **e**, Largest gross BG loss. **f**, Largest gross BG gain. The bottom colour bar is consistent across biomes (**c–f**) and cover types. Long-term gross dynamics of TC, SV and BG changes vary considerably between biomes. See Extended Data Fig. 2 for other biomes and Extended Data Table 2 for change area estimates.

continental scale, land-use activities account for the majority of observed land changes in Europe (86%), South America (66%), Asia (62%) and Africa (50%), but have a smaller role in North America (47%) and Oceania (35%). The specific land-change drivers are diverse, multi-scale and interactive[1], as discussed in detail below. However, changes collectively induced by the various drivers at the global scale appear to have been gradual over time (Extended Data Fig. 5).

Expansion of the agricultural frontier is the primary driver of deforestation in the tropics[10]. The three countries with the largest area of net tree cover loss during 1982–2016 are all located in South America: Brazil (−385,000 km^2, −8%), Argentina (−113,000 km^2, −25%) and Paraguay (−79,000 km^2, −34%) (Supplementary Table 1). The 'arc of deforestation' along the southeastern edge of the Amazon has been well-documented[7,10]. Clearing of natural vegetation for export-oriented industrial agriculture also prevailed in the Cerrado (Fig. 4a) and the Gran Chaco (Fig. 4b). Spatially clustered hotspots of deforestation are also found in Queensland, Australia, and in Southeast Asia—including Myanmar, Vietnam, Cambodia and Indonesia—diminishing the already scarce primary forests of the region[11]. In sub-Saharan Africa, tree cover loss was pervasive across the Congolian rainforests and the Miombo woodlands (Fig. 4c), historically related to smallholder agriculture and increasingly to commodity crop cultivation[12]. Forests in boreal Canada, eastern Alaska and central Siberia exhibited large patches of tree canopy loss and short vegetation gain, similar to the tropics (Fig. 1b). However, these are the result of persistent disturbances from wildfires and subsequent recovery of natural vegetation[13].

Discernible effects of climate change on vegetation change are also revealed at regional scales. In the western United States (Fig. 4d), forests are suffering from increasing stress from insects, wildfires, heat and droughts due to regional warming[14]. But in the temperature-limited Arctic, warming is facilitating woody vegetation growth in northeastern Siberia, western Alaska and northern Quebec[15] (Fig. 4e). Land-use activities are rare in these boreal tundra and polar ecosystems, contributing less than 1% to observed land changes (Extended Data Fig. 3e). In water-limited savannahs in Central and West Africa (Fig. 4f), forest expansion and woody encroachment—observed both from space and in the field[16]—are probably driven by increases in precipitation and atmospheric carbon dioxide[17]. Extreme high-rainfall anomalies also contributed to the greening of the Sahel[17] (Fig. 4f). Altitudinal biome shift is also expected in a changing climate. Global treeline positions have been advancing since AD 1900 as a result of climate warming[18]. The aforementioned bare ground loss, short vegetation loss and tree canopy gain in global mountain systems further suggest that an enduring transformation is occurring with regard to the distribution, structure and composition of montane vegetation.

Political, social and economic factors can influence vegetation in conjunction with climate drivers. Tree canopy in Europe, including European Russia, has increased by 35%—the greatest gain among all continents (Extended Data Table 1). Spatially contiguous hotspots of tree canopy gain were found in European Russia and Carpathian montane forests (Fig. 4g). Natural afforestation on abandoned agricultural land has been a common process in Eastern Europe after the collapse
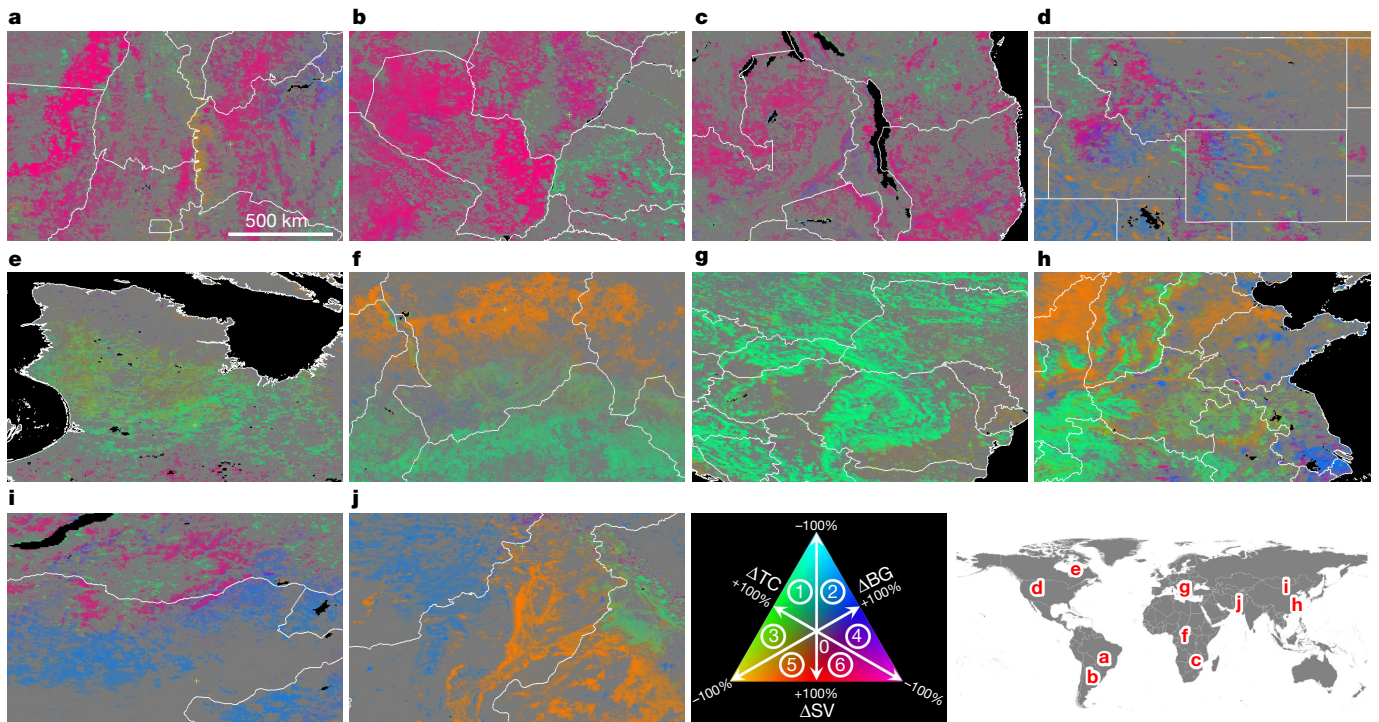
Fig. 4 | Regional subsets of changes in TC, SV and BG cover. As in Fig. 1b, pixels showing a statistically significant trend ($n = 35$, two-sided Mann–Kendall test, $P < 0.05$) in TC, SV or BG are depicted on the change map. **a**, Cerrado ecoregion in Brazil, centred at 11.4° S, 46.5° W. **b**, Gran Chaco ecoregion in Bolivia, Argentina and Paraguay, centred at 22.5° S, 55.7° W. **c**, Miombo woodlands in southeast Africa, centred at 12.4° S, 33.9° E. **d**, Western United States, centred at 44.5° N, 110.0° W. **e**, Quebec, Canada, centred at 57.9° N, 71.6° W. **f**, Central Africa, centred at 10.4° N, 19.4° E. **g**, Eastern Europe, centred at 46.1° N, 20.3° E. **h**, Eastern China, centred at 35.0° N, 115.1° E. **i**, Eastern Mongolia, centred at 48.7° N, 111.0° E. **j**, Afghanistan and Pakistan, centred at 30.7° N, 70.6° E. Circled numbers in the colour legend denote dominant change directions: 1, TC gain with SV loss; 2, BG gain with SV loss; 3, TC gain with BG loss; 4, BG gain with TC loss; 5, SV gain with BG loss; and 6, SV gain with TC loss.

of the Soviet Union[19]. Our satellite record confirms the effectiveness of China's large-scale reforestation and afforestation programs, particularly in the Loess Plateau and the Qin Ling–Daba Mountains[20] (Fig. 4h). An increasing area of plantations in southeastern China has also led to tree canopy gain (+34%) in China. Tree canopy also increased in the United States (+15%), mostly in the eastern United States (Fig. 1b). Unlike declining forest cover in the western United States (Fig. 4d), southeastern forests are recovering from historical disturbances or are under intensive forestry management[21].

The world's arid and semi-arid drylands exhibited large areas of decrease in short vegetation and large areas of increase in bare ground, indicating long-term land degradation. Hotspots of vegetation loss include the southwestern United States, southern Argentina, Kazakhstan, Mongolia (Fig. 4i), Inner Mongolia, China, Afghanistan (Fig. 4j) and large areas of Australia. The decrease in short vegetation cover in eastern Australia is probably the consequence of the long-term precipitation decline in the local growing season[22]. Rising surface temperatures, a reduction in rainfall, and overgrazing caused extensive grassland deterioration in the Mongolian steppe[23]. A nationwide ground survey in the United States revealed degradation of soils and vegetation combined with an increased dominance of invasive species in the southwest[24].

Human activities undoubtedly have a dominant role in agricultural and urban landscapes, where lands have been continually modified throughout human history. India and China had the largest bare ground loss among all countries (India, −270,000 km², −34%; China, −250,000 km², −7%). India also ranked second in short vegetation gain (+195,000 km², +9%), after Brazil (+396,000 km², +12%). While the short vegetation gain in Brazil is mainly due to the expansion of agricultural frontiers into natural ecosystems, short vegetation gain in India is primarily due to intensification of existing agricultural lands—a continuation of the 'Green Revolution'[25]. Some of the observed bare ground

gain can be attributed to resource extraction and urban sprawl, most notably in eastern China (Fig. 4h). However, at the global scale, the growth of urban areas accounts for a small fraction of all land changes[26].

Previous studies have found a greening Earth on the basis of trends in satellite-based vegetation properties (for example, leaf area index) and have linked this greening trend to a number of climatic and ecological factors[20,27–29]. A recent study[29] using ecosystem models attributed 70% of the observed increase in the global leaf area index to the CO_2 fertilization effect and 4% to land-use change. Our finding that global bare ground cover has decreased over the past 35 years suggests a net increase in vegetation cover and is thus consistent with the greening trend. However, our results differ from previous studies by quantifying the prominent role of land use in global vegetation change. Using a global probability-based sample, we attribute 60% of observed land changes to land-use activities (Extended Data Fig. 3). Our empirical approach is based on observations of high-resolution satellite data (Extended Data Fig. 4), avoiding the challenges of modelling the underlying drivers of land change[1]. Additionally, our TC–SV–BG land-cover product is thematically more advanced than vegetation indices in characterizing land surface change. For example, differentiating long-term changes in tree cover from other vegetation can facilitate an improved understanding of global fluxes of water, carbon and energy[9]. Our study provides observational evidence of increasing tree cover in northern continents, which may constitute the missing carbon sink[3]. By contrast, tropical tree cover loss is associated with higher biomass forests and is responsible for carbon emissions from deforestation[3,5]. These satellite-based trends are substantiated through the uncertainty analyses (Extended Data Fig. 6; see Supplementary Methods), with the caveat that the long-term field data that would be ideal for verifying historical land-cover change are not available.

The results of this study reflect a human-dominated Earth system. Direct human action on landscapes is found over large areas on every

continent, from intensification and extensification of agriculture to increases in forestry and urban land uses, with implications for the maintenance of ecosystem services[2]. However, human-induced climate change has been documented as an indirect cause of many of the quantified large-scale regional change dynamics, including woody encroachment in Arctic and montane systems and vegetation loss in semi-arid ecoregions[15,17,18,22,23,29]. Continuing land-use change and the increasing role of climate change in modifying land cover warrants continued monitoring of the Earth's land surface from space.

Reporting summary
Further information on experimental design is available in the Nature Research Reporting Summary linked to this paper.

Data availability
The AVHRR vegetation continuous fields products that we generated will be distributed through Land Processes Distributed Active Archive Center (LP DAAC, https://lpdaac.usgs.gov/dataset_discovery/measures/measures_products_table/vcf5kyr_v001). Vegetation continuous fields change and uncertainty layers are also provided at https://glad.umd.edu/dataset/long-term-global-land-change for download. All other data are available from the corresponding author upon reasonable request.

Online content
Any Methods, including any statements of data availability and Nature Research reporting summaries, along with any additional references and Source Data files, are available in the online version of the paper at https://doi.org/10.1038/s41586-018-0411-9.

1. Turner, B. L. II, Lambin, E. F. & Reenberg, A. The emergence of land change science for global environmental change and sustainability. *Proc. Natl Acad. Sci. USA* **104**, 20666–20671 (2007).
2. Foley, J. A. et al. Global consequences of land use. *Science* **309**, 570–574 (2005).
3. Le Quéré, C. et al. Global carbon budget 2016. *Earth Syst. Sci. Data* **8**, 605–649 (2016).
4. Alkama, R. & Cescatti, A. Biophysical climate impacts of recent changes in global forest cover. *Science* **351**, 600–604 (2016).
5. FAO. *Global Forest Resources Assessment 2015* (UN Food and Agriculture Organization, Rome, 2015).
6. Bonan, G. B. & Doney, S. C. Climate, ecosystems, and planetary futures: The challenge to predict life in Earth system models. *Science* **359**, eaam8328 (2018).
7. Hansen, M. C. et al. High-resolution global maps of 21st-century forest cover change. *Science* **342**, 850–853 (2013).
8. Feng, M. et al. Earth science data records of global forest cover and change: assessment of accuracy in 1990, 2000, and 2005 epochs. *Remote Sens. Environ.* **184**, 73–85 (2016).
9. DeFries, R. S. et al. Mapping the land surface for global atmosphere–biosphere models: toward continuous distributions of vegetation's functional properties. *J. Geophys. Res.* **100**, 20867–20882 (1995).
10. Gibbs, H. K. et al. Tropical forests were the primary sources of new agricultural land in the 1980s and 1990s. *Proc. Natl Acad. Sci. USA* **107**, 16732–16737 (2010).
11. Margono, B. A., Potapov, P. V., Turubanova, S., Stolle, F. & Hansen, M. C. Primary forest cover loss in Indonesia over 2000–2012. *Nat. Clim. Change* **4**, 730–735 (2014).
12. Ordway, E. M., Asner, G. P. & Lambin, E. F. Deforestation risk due to commodity crop expansion in sub-Saharan Africa. *Environ. Res. Lett.* **12**, 044015 (2017).
13. Hicke, J. A. et al. Postfire response of North American boreal forest net primary productivity analyzed with satellite observations. *Glob. Change Biol.* **9**, 1145–1157 (2003).
14. van Mantgem, P. J. et al. Widespread increase of tree mortality rates in the western United States. *Science* **323**, 521–524 (2009).
15. McManus, K. M. et al. Satellite-based evidence for shrub and graminoid tundra expansion in northern Quebec from 1986 to 2010. *Glob. Change Biol.* **18**, 2313–2323 (2012).
16. Mitchard, E. T. & Flintrop, C. M. Woody encroachment and forest degradation in sub-Saharan Africa's woodlands and savannas 1982–2006. *Phil. Trans. R. Soc. Lond. B* **368**, 20120406 (2013).
17. Brandt, M. et al. Human population growth offsets climate-driven increase in woody vegetation in sub-Saharan Africa. *Nat. Ecol. Evol.* **1**, 0081 (2017).
18. Harsch, M. A., Hulme, P. E., McGlone, M. S. & Duncan, R. P. Are treelines advancing? A global meta-analysis of treeline response to climate warming. *Ecol. Lett.* **12**, 1040–1049 (2009).
19. Potapov, P. V. et al. Eastern Europe's forest cover dynamics from 1985 to 2012 quantified from the full Landsat archive. *Remote Sens. Environ.* **159**, 28–43 (2015).
20. Piao, S. et al. Detection and attribution of vegetation greening trend in China over the last 30 years. *Glob. Change Biol.* **21**, 1601–1609 (2015).
21. Birdsey, R., Pregitzer, K. & Lucier, A. Forest carbon management in the United States: 1600–2100. *J. Environ. Qual.* **35**, 1461–1469 (2006).
22. Donohue, R. J., McVicar, T. R. & Roderick, M. L. Climate-related trends in Australian vegetation cover as inferred from satellite observations, 1981–2006. *Glob. Change Biol.* **15**, 1025–1039 (2009).
23. Liu, Y. Y. et al. Changing climate and overgrazing are decimating Mongolian steppes. *PLoS ONE* **8**, e57599 (2013).
24. Herrick, J. E. et al. National ecosystem assessments supported by scientific and local knowledge. *Front. Ecol. Environ.* **8**, 403–408 (2010).
25. Evenson, R. E. & Gollin, D. Assessing the impact of the green revolution, 1960 to 2000. *Science* **300**, 758–762 (2003).
26. Ying, Q. et al. Global bare ground gain from 2000 to 2012 using Landsat imagery. *Remote Sens. Environ.* **194**, 161–176 (2017).
27. Myneni, R. B., Keeling, C. D., Tucker, C. J., Asrar, G. & Nemani, R. R. Increased plant growth in the northern high latitudes from 1981 to 1991. *Nature* **386**, 698–702 (1997).
28. Forkel, M. et al. Codominant water control on global interannual variability and trends in land surface phenology and greenness. *Glob. Change Biol.* **21**, 3414–3435 (2015).
29. Zhu, Z. et al. Greening of the Earth and its drivers. *Nat. Clim. Change* **6**, 791–795 (2016).
30. FAO. *Global Ecological Zoning for the Global Forest Resources Assessment 2000* http://www.fao.org/docrep/006/ad652e/ad652e00.htm (UN Food and Agriculture Organization, Rome, 2001).

Extended Data Fig. 1 | Satellite-derived, long-term (1982–2016) changes in land cover show strong coupling and symmetry in change detection. **a**, Global map of co-located ΔTC and ΔSV. Pixels showing a statistically significant trend ($n = 35$ years, two-sided Mann–Kendall test, $P < 0.05$) in both TC and SV are depicted on the map. **b**, Global map of co-located ΔTC and ΔBG. **c**, Global map of co-located ΔSV and ΔBG. **d**, From left to right, intensity plot of change area for ΔTC versus ΔSV, ΔTC versus ΔBG and ΔSV versus ΔBG, corresponding to **a**, **b** and **c**, respectively. To create these intensity plots, paired per cent change layers (Fig. 1b) are used to construct a 2D histogram with bin size of 1% for both axes. Then, the total change area in each bin is calculated and plotted.
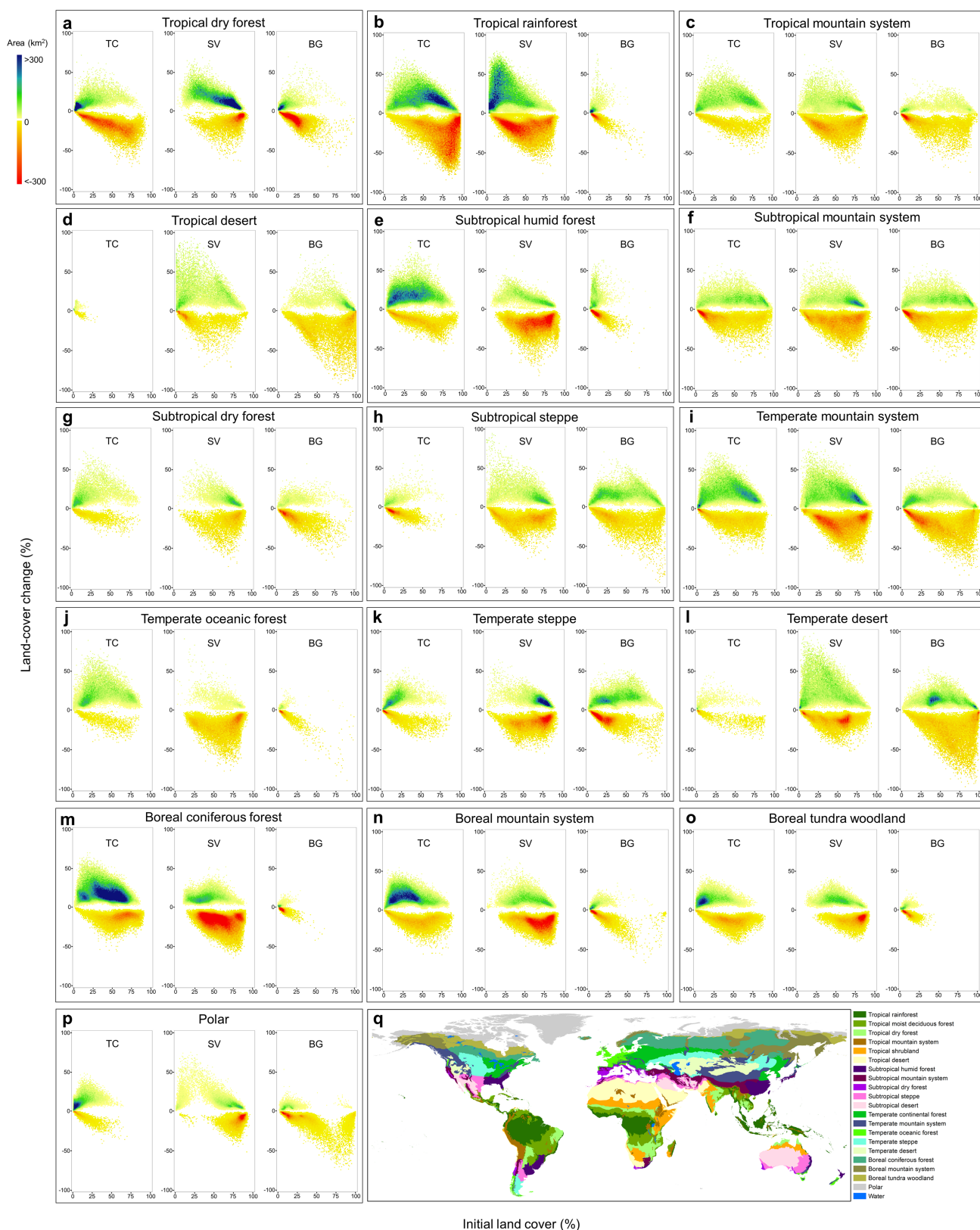
Extended Data Fig. 2 | Long-term (1982–2016) gross land-change dynamics vary considerably between biomes. a–p, Gross land-change dynamics per biome. Mountain systems (**c, f, i, n**) all exhibit larger area of TC gain than TC loss, larger area of SV loss than SV gain and larger area of BG loss than BG gain. **q**, Geographical distribution of all biomes, from a previous publication[30], reproduced with permission. See Fig. 3 for other biomes and Extended Data Table 2 for change area estimates.

c

Land-cover change type	DHI (SE)	n
Global average (all changes)	60 (1)	1,500
TC gain	66 (3)	250
TC loss	70 (3)	250
SV gain	61 (3)	250
SV loss	55 (3)	250
BG gain	36 (3)	250
BG loss	62 (3)	250

d

Continent	DHI (SE)	n
Africa	50 (3)	222
Asia	62 (2)	529
Europe	86 (3)	146
North America	47 (3)	239
South America	66 (3)	277
Oceania	35 (5)	87

e

Biome	DHI (SE)	n	Biome	DHI (SE)	n
Tropical rainforest	71 (4)	160	Subtropical desert	23 (5)	69
Tropical moist deciduous forest	69 (4)	171	Temperate continental forest	87 (3)	102
Tropical dry forest	66 (4)	112	Temperate mountain system	56 (5)	109
Tropical mountain system	60 (7)	46	Temperate oceanic forest	77 (8)	28
Tropical shrubland	61 (5)	110	Temperate steppe	67 (5)	75
Tropical desert	62 (11)	19	Temperate desert	42 (6)	65
Subtropical humid forest	92 (3)	77	Boreal coniferous forest	52 (5)	83
Subtropical mountain system	57 (6)	61	Boreal mountain system	6 (3)	66
Subtropical dry forest	78 (8)	27	Boreal tundra woodland	0 (0)	29
Subtropical steppe	54 (6)	71	Polar	1 (2)	20

Extended Data Fig. 3 | Attributing direct human impact versus indirect drivers to detected changes in land cover. Indirect drivers include both natural drivers and human-induced climate change. **a**, Spatial distribution of the probability sample used for the attribution estimates ($n = 1,500$). **b**, Direct human impact (DHI) of each sample unit interpreted using a time-series of high-resolution images in Google Earth. **c**, Estimated DHI as a per cent of all change area at the global scale. Global average is calculated by weighting the human impact of each type by each respective global total area provided in Extended Data Table 1. The standard error (SE) for the estimated per cent of DHI is provided in the parentheses. **d**, **e**, Estimated DHI at the continental and biome scales. See Extended Data Fig. 4 for some representative sample examples.
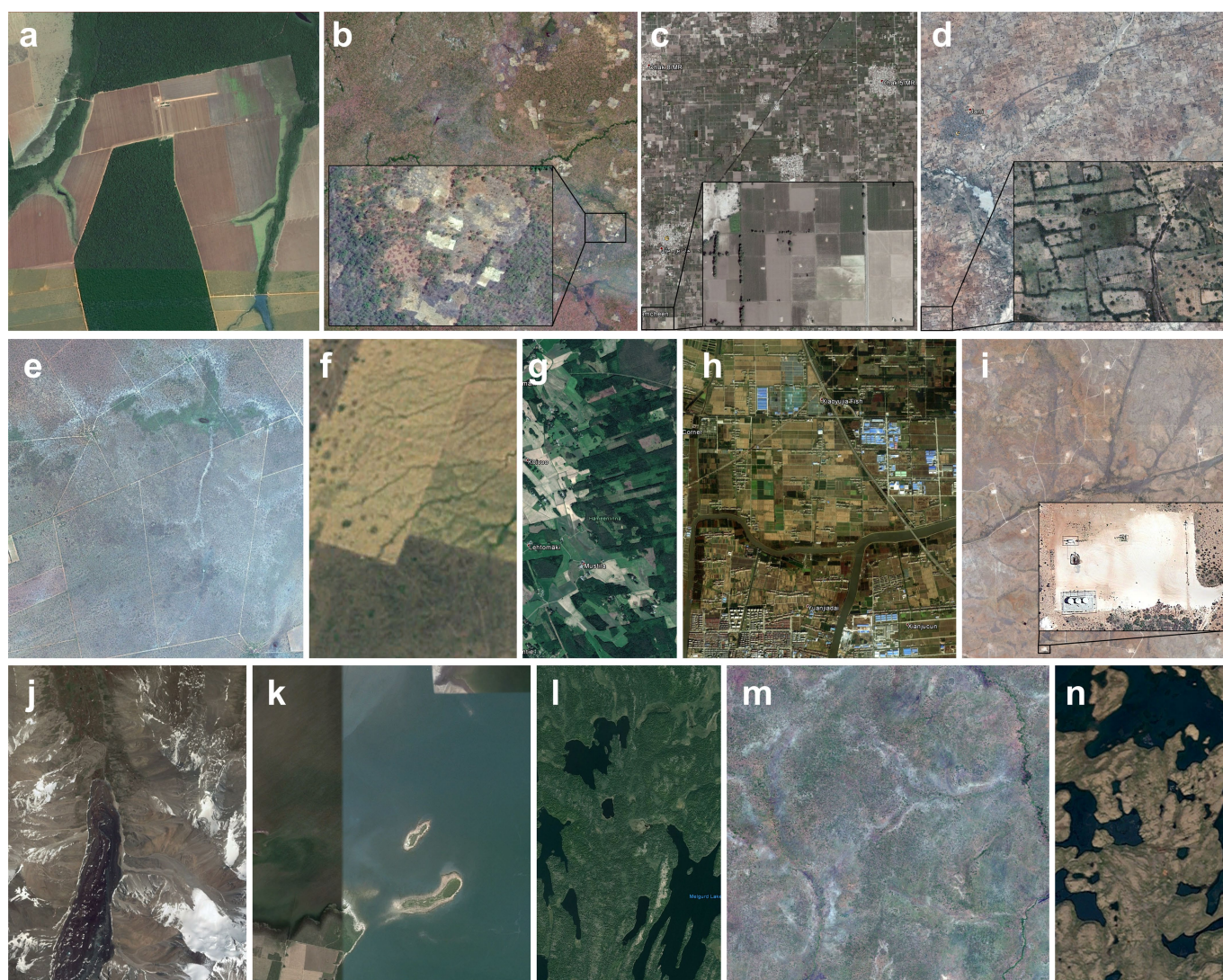
Extended Data Fig. 4 | Selected sample examples for driver attribution. Screenshots are taken from Google Earth. Each panel is 0.05° × 0.05° in size, corresponding to one AVHRR pixel. **a**, Deforestation for industrial agriculture expansion in Mato Grosso, Brazil (11.275° S, 52.125° W). **b**, Expanding shifting agriculture in northern Zambia (11.625° S, 28.625° E). **c**, Intensification of small-holder agriculture in Punjab, Pakistan (30.025° N, 71.675° E). **d**, Short vegetation gain in low-intensity agricultural lands in northern Nigeria (12.825° N, 7.825° E). **e**, Short vegetation increase due to effective fire suppression in pasture lands in Omaheke, Namibia[31] (22.175° S, 18.925° E). **f**, Managed pasture lands in western Kazakhstan (49.475° N, 47.725° E). **g**, Forestry in southern Finland (61.075° N, 24.475° E). **h**, Urbanization in Shanghai, China (30.925° N, 121.175° E). **i**, Oil extraction in New Mexico, USA (32.875° N, 104.275° W). **j**, Herbaceous vegetation increase owing to glacial retreat in Chuy, Kyrgyzstan (42.575° N, 74.775° E). **k**, Bare ground cover variation along Mar Chiquita lake shore in Cordoba, Argentina (30.675° S, 63.025° W). **l**, Forest fires in Saskatchewan, Canada (55.225° N, 102.225° W). **m**, Tree cover increase in unpopulated savannahs in Western Equatoria, South Sudan[16,17] (6.575° N, 27.725° E). **n**, Climate-change-driven woody encroachment in Quebec, Canada[15] (59.475° N, 73.225° W). Examples **a**–**i** show various types of land use, whereas examples **j**–**n** do not show visible signs of human activity. Map data: Google, DigitalGlobe, CNES/Airbus, Landsat/Copernicus.

31. Gessner, U., Machwitz, M., Conrad, C. & Dech, S. Estimating the fractional cover of growth forms and bare surface in savannas. A multi-resolution approach based on regression tree ensembles. *Remote Sens. Environ.* **129**, 90–102 (2013).
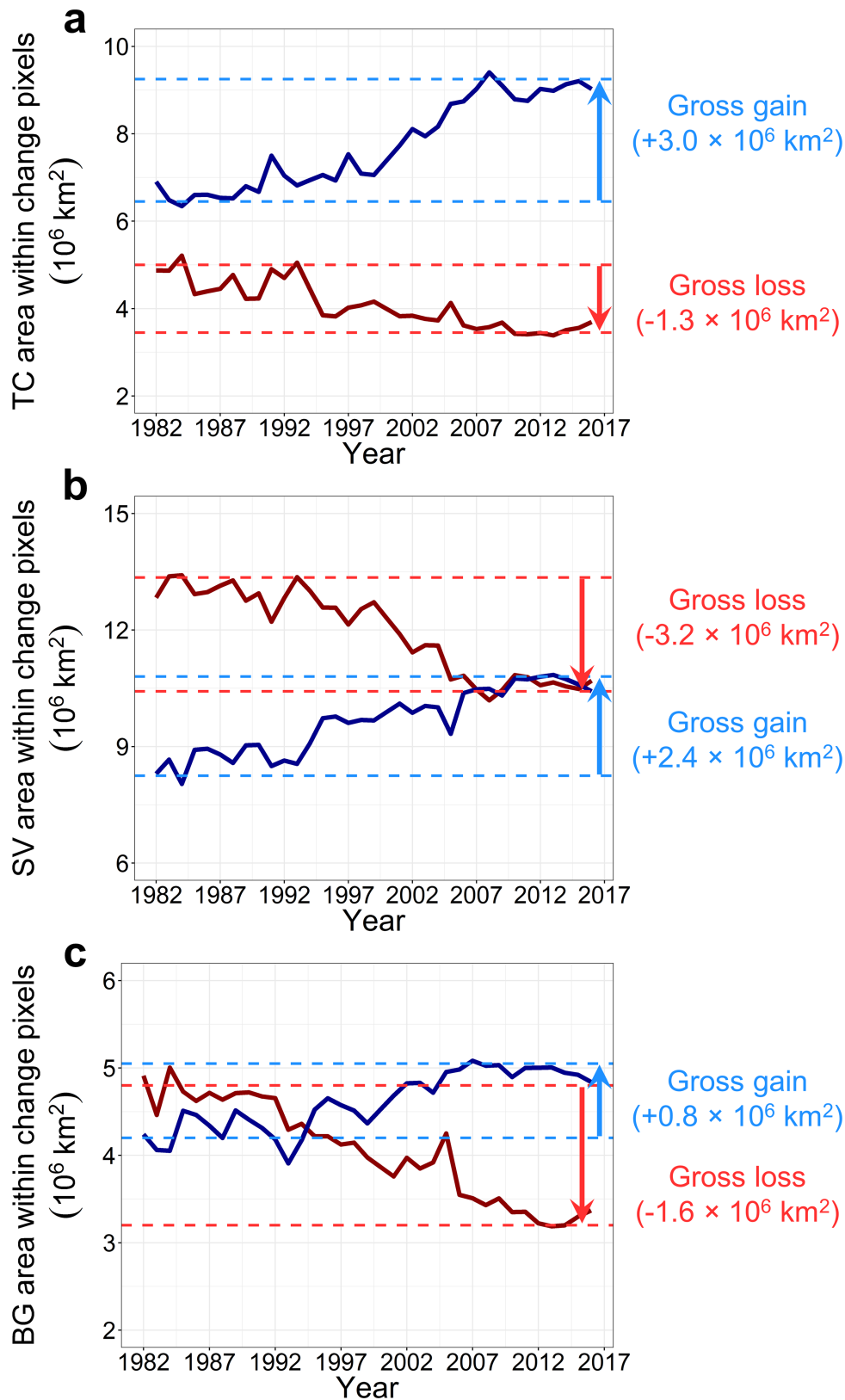
Extended Data Fig. 5 | Global trends in land cover during 1982–2016.
a, Trends in TC cover. **b**, Trends in SV cover. **c**, Trends in BG cover. The
following steps were taken for each cover type using TC as the example.
The TC gain layer (Fig. 1b) was overlaid on the annual TC% stack to
compute annual global TC area within the gain mask (solid dark blue
lines); the TC loss layer (Fig. 1b) was overlaid on the annual TC% stack

to compute annual global TC area within the loss mask (solid dark red
lines). Gross gain estimates from 1986 to 2016 are marked by blue arrows
and dashed lines; gross loss estimates from 1986 to 2016 are marked by red
arrows and dashed lines. See Extended Data Table 1 for exact gross change
estimates.
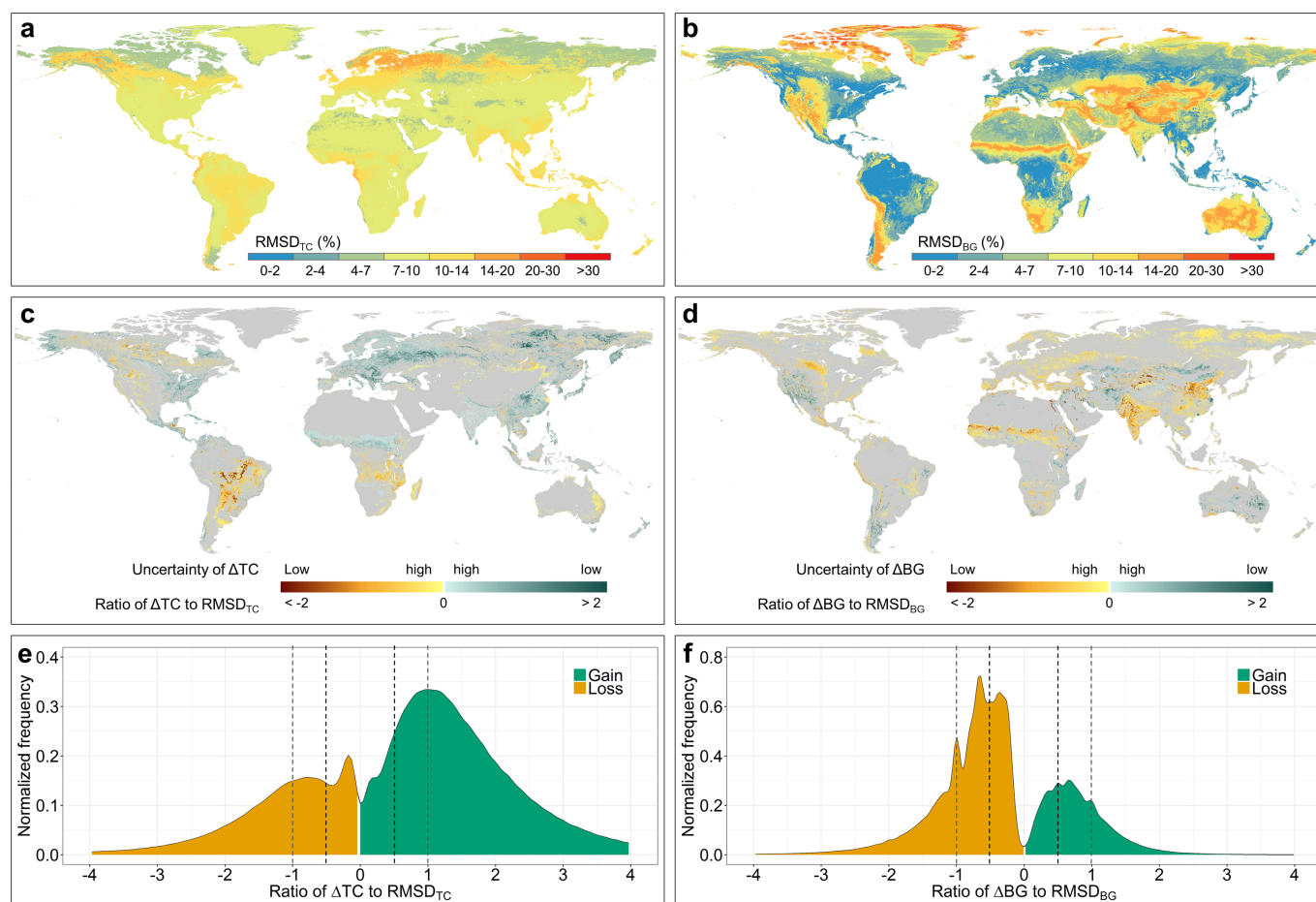
Extended Data Fig. 6 | Uncertainty of ΔTC and ΔBG. a, Spatial distribution of annual mean root-mean-square-deviation (RMSD) of TC between 1982 and 2016. **b**, Spatial distribution of annual mean RMSD of BG between 1982 and 2016. **c**, Spatial distribution of ΔTC uncertainty. **d**, Spatial distribution of ΔBG uncertainty. **e**, Normalized frequency distribution of ΔTC uncertainty. **f**, Normalized frequency distribution of ΔBG uncertainty. TC, BG and associated RMSD values are outputs of regression tree models. Uncertainty is represented by the ratio of long-term TC (or BG) change estimates to respective RMSD estimates. Positive values of the ratio metric represent the uncertainties of gains and negative values represent the uncertainties of losses. A greater absolute value indicates lower uncertainty, and vice versa. Area under the frequency distribution equals 1. The frequency distributions suggest that tree cover gain exceeds tree cover loss and bare ground loss exceeds bare ground gain for any threshold level (for example, dashed lines), hence the observed trends (a net gain in tree cover and a net loss in bare ground cover over the study period) are valid.

Extended Data Table 1 | Estimates of 1982 land-cover area and 1982–2016 land-cover change at continental and global scales

Continent	Tree canopy cover							Short vegetation cover							Bare ground cover						
		Annual net change				Gross change			Annual net change				Gross change			Annual net change				Gross change	
	Area 1982 (10^3 km^2)	Slope (10^3 km^2 yr^{-1})	Lower (10^3 km^2 yr^{-1})	Upper (10^3 km^2 yr^{-1})	p	loss (10^3 km^2)	gain (10^3 km^2)	Area 1982 (10^3 km^2)	Slope (10^3 km^2 yr^{-1})	Lower (10^3 km^2 yr^{-1})	Upper (10^3 km^2 yr^{-1})	p	loss (10^3 km^2)	gain (10^3 km^2)	Area 1982 (10^3 km^2)	Slope (10^3 km^2 yr^{-1})	Lower (10^3 km^2 yr^{-1})	Upper (10^3 km^2 yr^{-1})	p	loss (10^3 km^2)	gain (10^3 km^2)
Africa	4672	-1.9	-7.6	3.6	0.609	-267	262	11653	14.8	6.5	23.2	0.016	-268	571	13413	-12.4	-19.9	-4.7	0.020	-371	105
Asia	8457	37.5	28.0	45.3	0.000	-178	1170	21774	-22.9	-34.5	-9.6	0.008	-1261	760	13926	-15.1	-23.1	-7.4	0.002	-798	358
Europe	2719	28.3	20.4	32.8	0.000	-17	758	6320	-22.0	-27.3	-14.7	0.000	-673	50	668	-4.3	-5.8	-2.6	0.000	-92	9
North America	5815	15.6	3.5	24.2	0.020	-205	583	12921	-12.7	-4.1	-2.2	0.031	-594	286	4847	-2.5	-7.3	2.2	0.363	-186	140
South America	8767	-14.1	-20.5	-7.4	0.001	-621	190	7165	14.8	8.1	21.0	0.002	-224	655	1717	1.9	-1.2	3.8	0.307	-92	102
Oceania	680	0.1	-1.4	1.7	0.887	-40	56	4600	-4.4	-12.1	3.4	0.349	-132	50	2772	5.2	-3.9	12.5	0.280	-35	113
Global	31628	66.0	27.3	100.5	0.008	-1331	3039	64539	-26.0	-64.8	15.2	0.244	-3170	2380	37412	-34.0	-52.3	-10.0	0.023	-1582	830

Annual net change in land cover (slope) and 1982 land-cover area were estimated using Theil–Sen regression of the time series of annual land-cover area per continent or over the globe (excluding Antarctica). Lower and upper slopes represent the 90% confidence interval. Reported P value is for the two-sided Mann–Kendall test for trend, with $P < 0.05$ used to define statistical significance, and a sample size of $n = 35$ years. Gross change in land cover was estimated on the basis of per-pixel non-parametric trend analysis. Per-pixel loss and gain were summed to derive gross loss and gain at the aggregated scales.

Extended Data Table 2 | Estimates of 1982 land-cover area and 1982–2016 land-cover change at biome and climate zone scales

Biome / climate zone	Tree canopy cover							Short vegetation cover							Bare ground cover						
	Area 1982 (10³ km²)	Annual net change				Gross change		Area 1982 (10³ km²)	Annual net change				Gross change		Area 1982 (10³ km²)	Annual net change				Gross change	
		Slope (10³ km² yr⁻¹)	Lower (10³ km² yr⁻¹)	Upper (10³ km² yr⁻¹)	p	loss (10³ km²)	gain (10³ km²)		Slope (10³ km² yr⁻¹)	Lower (10³ km² yr⁻¹)	Upper (10³ km² yr⁻¹)	p	loss (10³ km²)	gain (10³ km²)		Slope (10³ km² yr⁻¹)	Lower (10³ km² yr⁻¹)	Upper (10³ km² yr⁻¹)	p	loss (10³ km²)	gain (10³ km²)
Tropical rainforest	10519	-1.9	-4.4	1.6	0.443	-332	315	3721	2.1	-1.0	5.1	0.307	-292	326	236	-0.4	-0.7	-0.1	0.025	-19	15
Tropical moist deciduous forest	3569	-2.5	-8.5	2.2	0.460	-373	285	6912	5.8	0.3	10.9	0.078	-236	386	492	-2.2	-3.0	-1.3	0.001	-71	29
Tropical dry forest	1236	-2.8	-5.1	-1.1	0.018	-184	99	5386	7.2	4.0	10.2	0.001	-70	246	821	-3.8	-5.9	-1.9	0.010	-121	32
Tropical mountain system	1333	3.5	2.4	4.5	0.000	-23	118	2092	-1.4	-3.1	0.2	0.118	-106	65	1092	-1.7	-2.7	-0.9	0.002	-61	17
Tropical shrubland	149	0.3	-0.2	0.7	0.349	-15	20	4010	12.3	6.8	18.5	0.001	-41	371	4137	-12.0	-19.0	-6.1	0.003	-379	43
Tropical desert	19	0.0	0.0	0.0	0.532	0	1	692	1.6	0.2	3.4	0.061	-31	87	10846	-1.5	-3.4	-0.1	0.057	-88	31
Tropical climate zone	16837	-4.1	-14.4	3.6	0.320	-927	837	22691	30.0	14.7	43.0	0.002	-775	1480	17617	-25.5	-34.7	-12.0	0.002	-740	167
Subtropical humid forest	1566	8.2	4.4	12.0	0.002	-48	268	2866	-7.3	-10.5	-3.7	0.003	-236	46	196	-0.7	-1.4	-0.3	0.012	-38	22
Subtropical mountain system	516	3.1	2.3	3.8	0.000	-20	116	2571	-2.8	-4.3	-1.2	0.008	-153	68	1756	0.0	-1.7	1.8	0.932	-79	79
Subtropical dry forest	198	1.6	0.9	2.3	0.001	-8	49	1107	0.2	-0.5	0.8	0.755	-37	33	266	-1.2	-1.9	-0.6	0.002	-45	10
Subtropical steppe	179	-0.8	-2.0	0.2	0.191	-27	12	2594	-1.4	-4.2	1.8	0.460	-84	64	2106	3.2	-0.9	6.7	0.201	-61	106
Subtropical desert	29	-0.2	-0.4	0.0	0.118	-3	2	2606	-4.4	-10.3	1.3	0.233	-128	45	4001	4.5	-1.3	10.6	0.233	-46	133
Subtropical climate zone	2453	12.1	6.5	16.8	0.004	-105	448	11741	-14.0	-23.1	-5.6	0.013	-639	257	8323	5.6	-6.8	17.0	0.443	-269	350
Temperate continental forest	2172	21.4	15.1	26.0	0.000	-11	591	4451	-17.9	-22.5	-11.3	0.000	-528	28	277	-2.7	-3.4	-2.2	0.000	-61	7
Temperate mountain system	1552	5.9	3.6	7.4	0.001	-53	198	3459	-2.0	-4.0	0.5	0.211	-213	172	2175	-2.9	-5.1	-1.1	0.023	-161	62
Temperate oceanic forest	551	3.8	2.1	5.3	0.001	-6	101	1162	-3.3	-4.9	-1.8	0.003	-92	8	61	-0.4	-0.5	-0.2	0.000	-8	2
Temperate steppe	320	2.2	0.1	3.4	0.069	-18	56	4191	-2.9	-6.7	0.0	0.105	-130	72	1338	2.3	-1.5	5.8	0.363	-86	108
Temperate desert	61	-0.1	-0.2	0.1	0.514	-5	4	1661	-0.3	-2.9	3.5	0.955	-101	135	3642	0.3	-3.6	3.1	0.887	-135	103
Temperate climate zone	4681	33.5	21.0	41.9	0.000	-92	951	14814	-24.3	-37.3	-12.2	0.006	-1064	414	7491	-4.3	-14.0	1.8	0.268	-451	282
Boreal coniferous forest	3938	13.6	6.7	18.7	0.003	-75	415	4239	-12.6	-17.1	-6.3	0.002	-369	71	205	-1.4	-1.8	-0.9	0.001	-23	2
Boreal mountain system	2035	6.6	3.9	9.9	0.005	-61	225	3909	-6.2	-8.8	-3.3	0.003	-193	64	341	-1.2	-1.7	-0.6	0.002	-33	11
Boreal tundra woodland	971	1.3	-1.5	3.7	0.363	-58	82	2723	-0.9	-2.9	1.2	0.478	-63	52	228	-0.7	-1.2	-0.2	0.044	-16	5
Boreal climate zone	6796	21.0	7.9	31.0	0.009	-194	723	10857	-20.3	-27.5	-11.7	0.002	-625	187	772	-3.4	-4.5	-2.2	0.001	-71	19
Polar	236	2.2	0.9	3.1	0.009	-7	55	4109	0.4	-1.3	2.1	0.712	-43	30	3080	-2.6	-3.6	-1.1	0.010	-41	8

Consistent with Extended Data Table 1, annual net change in land cover (slope) and 1982 land-cover area were estimated using Theil–Sen regression of the time series of annual land-cover area per biome or climate zone. Lower and upper slopes represent the 90% confidence interval. Reported P value is for the two-sided Mann–Kendall test for trend with $P < 0.05$ used to define statistical significance and a sample size of $n = 35$ years. Gross change in land cover was estimated on the basis of per-pixel non-parametric trend analysis. Per-pixel loss and gain were summed to derive gross loss and gain at the aggregated scales. See Extended Data Fig. 2q for the geographical distribution of biomes.

naturereserch

Corresponding author(s):   Xiao-Peng Song

Reporting Summary

Nature Research wishes to improve the reproducibility of the work that we publish. This form provides structure for consistency and transparency in reporting. For further information on Nature Research policies, see Authors & Referees and the Editorial Policy Checklist.

Statistical parameters

When statistical analyses are reported, confirm that the following items are present in the relevant location (e.g. figure legend, table legend, main text, or Methods section).

n/a	Confirmed	
☐	☒	The exact sample size (*n*) for each experimental group/condition, given as a discrete number and unit of measurement
☐	☒	An indication of whether measurements were taken from distinct samples or whether the same sample was measured repeatedly
☐	☒	The statistical test(s) used AND whether they are one- or two-sided *Only common tests should be described solely by name; describe more complex techniques in the Methods section.*
☒	☐	A description of all covariates tested
☐	☒	A description of any assumptions or corrections, such as tests of normality and adjustment for multiple comparisons
☐	☒	A full description of the statistics including central tendency (e.g. means) or other basic estimates (e.g. regression coefficient) AND variation (e.g. standard deviation) or associated estimates of uncertainty (e.g. confidence intervals)
☐	☒	For null hypothesis testing, the test statistic (e.g. *F*, *t*, *r*) with confidence intervals, effect sizes, degrees of freedom and *P* value noted *Give P values as exact values whenever suitable.*
☒	☐	For Bayesian analysis, information on the choice of priors and Markov chain Monte Carlo settings
☒	☐	For hierarchical and complex designs, identification of the appropriate level for tests and full reporting of outcomes
☐	☒	Estimates of effect sizes (e.g. Cohen's *d*, Pearson's *r*), indicating how they were calculated
☐	☒	Clearly defined error bars *State explicitly what error bars represent (e.g. SD, SE, CI)*

Our web collection on statistics for biologists may be useful.

Software and code

Policy information about availability of computer code

Data collection	Sample-based driver attribution data were collected using Google Earth (freely available at https://www.google.com/earth/)
Data analysis	The regression tree algorithm used to generate VCF layers was developed by Breiman et al. (1984). An R implementation is freely available at https://cran.r-project.org/web/packages/rpart/. Land-cover change characterization was implemented in Python using the Mann-Kendall-Trend package (freely available on GitHub at https://github.com/mps9506/Mann-Kendall-Trend), the SciPy library (freely available at https://www.scipy.org/) and the GDAL library (freely available at http://www.gdal.org/). Visualization maps were created using ArcMap 10.2.2 and PCI Geomatica 2014.

For manuscripts utilizing custom algorithms or software that are central to the research but not yet described in published literature, software must be made available to editors/reviewers upon request. We strongly encourage code deposition in a community repository (e.g. GitHub). See the Nature Research guidelines for submitting code & software for further information.

Data

All manuscripts must include a data availability statement. This statement should provide the following information, where applicable:

- Accession codes, unique identifiers, or web links for publicly available datasets
- A list of figures that have associated raw data
- A description of any restrictions on data availability

The generated AVHRR VCF products will be distributed through Land Processes Distributed Active Archive Center (LP DAAC, https://lpdaac.usgs.gov/). VCF change and uncertainty layers are also provided at http://glad.geog.umd.edu/dataset/long-term-global-land-change for download.

Field-specific reporting

Please select the best fit for your research. If you are not sure, read the appropriate sections before making your selection.

☐ Life sciences   ☐ Behavioural & social sciences   ☒ Ecological, evolutionary & environmental sciences

For a reference copy of the document with all sections, see nature.com/authors/policies/ReportingSummary-flat.pdf

Ecological, evolutionary & environmental sciences study design

All studies must disclose on these points even when the disclosure is negative.

Study description	This study mapped annual global land cover between 1982 and 2016 using satellite data and quantified land-cover change over the study period.
Research sample	Two separate probability samples were selected, one used for land cover validation and one used for the driver attribution analysis. The validation sample used existing datasets described in Olofsson et al. (2012), Stehman et al. (2012) and Pengra et al. (2015) (available at https://landcover.usgs.gov/glc/SitesDescriptionAndDownloads.php). The population from which the validation sample was selected was the global land surface. The driver attribution sample used high-resolution satellite images from Google Earth. The population represented by the driver attribution sample was the global land-cover change area.
Sampling strategy	A complete description of the sampling design for the validation sample is available in Olofsson et al. (2012) and Stehman et al. (2012). For the driver attribution sample, an a priori sample size calculation was not employed. An initial sample size of 300 was selected and reported in the original submission. Upon reviewing the standard errors for the estimated proportion of change attributable to land use, we increased the sample size to 1500. The standard errors reported in the revised manuscript are accordingly much smaller, but this sample size was not chosen based on a formal sample size planning calculation.
Data collection	A complete description of data collection for the validation sample is available in Pengra et al. (2015). For the driver attribution sample, data were collected by the authors via visualizing high-resolution images in Google Earth.
Timing and spatial scale	The timing of the validation sample ranges from year 2002 to 2014. The spatial scale of the validation sample data is 5-km x 5-km. The timing of the driver attribution sample ranges from year 1982 to 2016. The spatial scale of the driver attribution sample is 0.05 degree x 0.05 degree.
Data exclusions	No data were excluded from analysis.
Reproducibility	Our study did not involve comparisons of treatment groups or populations so we did not employ traditional experimental design and analysis of variance techniques. Consequently replication of experimental units is not applicable to our study design. The reliability of our findings was evaluated based on the reported uncertainty analyses, the accuracy assessment results, and the standard errors accompanying sample-based estimates.
Randomization	Randomization was incorporated in the sample selection process following standard protocols of probability sampling design.
Blinding	The typical use of "blinding" observers to the identity of treatment and control groups was not applicable in our study. However, a similar concept of "blinding" was incorporated in our accuracy assessment work as the interpreters collecting the reference condition data for comparison to the map classification did not know the map label for the sample units being interpreted.

Did the study involve field work?   ☐ Yes   ☒ No

Reporting for specific materials, systems and methods

Materials & experimental systems

n/a	Involved in the study
☒	Unique biological materials
☒	Antibodies
☒	Eukaryotic cell lines
☒	Palaeontology
☒	Animals and other organisms
☒	Human research participants

Methods

n/a	Involved in the study
☒	ChIP-seq
☒	Flow cytometry
☒	MRI-based neuroimaging